

Quantum machines based on Cu_3 -like compounds using the Heisenberg antiferromagnetic model in a triangular ring

Onofre Rojas¹ and Moises Rojas¹

¹*Department of Physics, Institute of Natural Science,
Federal University of Lavras, 37200-900 Lavras-MG, Brazil*

In this work, we present a theoretical investigation into an antiferromagnetically coupled spin system, specifically $\text{Cu}_3 - \text{X}(\text{X}=\text{As}, \text{Sb})$, which exhibits a configuration of a slightly distorted equilateral triangle, as identified in previous literature. This system is modeled using the Heisenberg model within a triangular structure, incorporating exchange interaction, Dzyaloshinskii-Moriya interaction, g-factors, and an external magnetic field. We explore three quantum machines based on the Cu_3 -like antiferromagnetically coupled spin system. The magnetocaloric effect (MCE), which is notably more significant at low temperatures, around $T \sim 1\text{K}$, for a perpendicular magnetic field at approximately $\sim 5\text{T}$, has been analyzed. We examine the Carnot machine, observing the influence of the external magnetic field on its operation as both a heat engine and refrigerator, and discuss the thermal efficiencies under these conditions. Our findings suggest that enhanced MCE allows for broader operation regions as a heat engine. Additionally, we explore the quantum Otto machine, showing its versatility in functioning as a heat engine, refrigerator, heater, and thermal accelerator. However, it mainly operates as a refrigerator and accelerator. We also explore their corresponding thermal efficiencies. Similarly, we have analyzed the quantum Stirling machine, which is capable of functioning as a heat engine, refrigerator, heater, and thermal accelerator, but it mainly operates as a refrigerator and thermal accelerator. We also examined the corresponding thermal efficiencies. It is worth mentioning that the Otto machine performance as a heat engine is notably influenced by the MCE, while the operational mode of the Stirling machine switches between a heat engine and accelerator around MCE is more prominent.

I. INTRODUCTION

In the past two decades, substantial efforts have been made by numerous researchers to explore new thermodynamic processes in realms where quantum features of matter play a significant role. This investigation has successfully integrated theoretical proposals [1] with experimental evidence [2], effectively narrowing the distance between the conceptual framework of quantum thermodynamics and its practical applications. Quantum heat engines, including the well-known Carnot and Otto engines, have been delineated and their characteristics compared to those of their classical equivalents. In addition, the analysis of a quantum model of a heat engine has showcased its efficiency and explored its irreversible nature [3, 4]. The construction and examination of entangled quantum heat engines have offered new insights into how entanglement affects thermodynamic efficiencies and other relevant quantities [5, 6], reaffirming the validity of the second law within this context [5]. Quantum thermodynamics has provided a coherent framework for understanding the operation and optimization of engines and refrigerators, thereby elucidating their functioning principles [7]. The study of quantum heat engines based on harmonic oscillators has further contributed to our understanding of optimization techniques and the concept of irreversibility [8, 9]. Demonstrated through experiments has revealed that a quantum-dot heat engine, which operates without mechanical parts, can nearly reach ideal efficiency levels, presenting a solid-state particle-exchange engine with high efficiency, pertinent to the advancement of future quantum technologies [10]. Furthermore, the

investigation on quantum thermal machines in a pair of coupled double quantum dots revealed the emergence of various operating regimes of the thermal machines[11].

Recent investigations have shed light on quantum Carnot, Otto, and Stirling engines, surpassing previous limitations in the pursuit of Carnot efficiency with quantum and nanoscale heat engines. These advancements include achieving Carnot efficiency through semi-local thermal operations by interacting with two baths simultaneously [12]. An analysis of a six-stroke irreversible quantum Carnot cycle revealed that inner friction significantly reduces work output and efficiency [13]. Studies comparing work extraction and efficiency in classical and quantum magnetic Otto cycles found classical cycles superior due to thermodynamic equilibrium [14]. Research on the Otto cycle's energy quantization effects showed enhanced performance, with proposals for experimental validation using trapped ions [15]. The reversible quantum Stirling cycle, involving single or coupled spin systems, was examined, unveiling the possibility of a heat engine transforming into a refrigerator under certain conditions [16]. Comparisons between quantum mechanical versions of Stirling and Otto cycles for interacting spin systems highlighted the quantum Stirling cycle's superiority in work production and operational range [17]. Furthermore, a quantum Stirling engine based on dinuclear metal complexes demonstrated tunable operational modes, offering potential applications in emerging quantum technologies [18]. In this sense, several works have focused on theoretical working substances as dimer systems. Some of these works include quantum machines operating as quantum engines, refrigerators, and heaters within a quantum Otto

cycle using coupled spins, as reported in references [19–22], and even including Dzyaloshinskii–Moriya interactions [23]. Although there are also theoretical investigations based on a single spin [24] as well as spin lattice systems [25], which have been extensively studied, but considering working substances as trimer systems have been rarely studied. One of the few works concerning a quantum Otto cycle with trimer systems has been analyzed in reference [26].

On the other hand, nanoscale materials exhibiting Giant Magnetocaloric Effect (GMCE) have drawn significant interest for their exceptional surface-to-volume ratio, intensified interactions, and swift thermal responses, making them ideal for temperature regulation in various applications. These include the development of a room-temperature thermal diode [27], an innovative self-pumping magnetic cooling device employing Mn-Zn ferrite nanoparticles for effective energy conservation without the need for external power [28], and a ferrofluid-based magnetic cooling system capable of transferring heat across extensive distances efficiently [29]. Additionally, the manipulation of ferrofluid droplets within microfluidic environments [30], and the investigation of magnetostructural phase transitions in Ni-Mn-Ga films, which exhibit a significant MCE at low magnetic fields [31], have been explored. Further applications extend to energy conversion using gadolinium thick films [32, 33], as well as in the biomedical field for magnetic hyperthermia treatments [34] and enhancing drug delivery through nanocarriers [35].

The exploration of magnetic materials has garnered widespread interest for their vast potential in advancing technologies within spintronics, nanoscale fabrication, and medical applications. Research into a Cu_3 nanomagnet has revealed phenomena such as half-step magnetization, hysteresis loops, and asymmetric magnetization, which are thought to be the result of adiabatic changes and Dzyaloshinskii–Moriya interactions (DMI) [36], while spin-electric coupling has been another focus of study [37]. Investigations into $S = 1/2$ spin triangle clusters have shown that their magnetization behavior and spin configurations are strongly influenced by the presence of a diamagnetic heteroatom ($X = \text{As}$ and Sb) [38], indicating their utility in the development of spin-based quantum gates [39]. A study on a spin-frustrated trinuclear copper complex using triaminoguanidine revealed significant antiferromagnetic interactions with minimal antisymmetric exchange [40], alongside research into various triangular copper structures [41–45]. Furthermore, $S = 1/2$ antiferromagnetic triangular spin rings have been identified as prime candidates for studying unique quantum magnetization effects, including unusual magnetization jumps in compounds such as spin-frustrated $(\text{VO})_3^{6+}$ -triangle-sandwiched octadecatungstates, which exhibit atypical magnetization steps [46]. Additionally, the antisymmetric exchange in a tri-copper(II) complex, has shedding light on its origins and theoretical implications, paving the way for advanced electronic structure

calculations [47].

Theoretical investigations aimed at delving into the intricate properties of nanomagnets or magnetic molecular clusters, which extend beyond what is observable in experiments, plays a crucial role. Insights from such research are documented extensively, with several noteworthy theoretical explorations highlighted in the literature [48–51]. Recently, theoretical investigation on the V_6 polyoxovanadate molecular magnet [48] employed numerical methods to reveal its highly adaptable magnetocaloric properties. In another study, the properties of spin-1/2 Hamiltonian in coupled isosceles Heisenberg triangles were examined through exact diagonalization, revealing a quantum phase transition diagram and magnetization characteristics at zero temperature, alongside their thermodynamic behavior and magnetocaloric effects [50]. Later, further investigation into a Cu_5 pentameric molecule using the spin-1/2 Heisenberg model shed light on its thermodynamic characteristics, phase transitions, magnetization, and magnetocaloric effects [51]. Karlova et al. focused on antiferromagnetic spin-1/2 XXZ Heisenberg clusters, uncovering additional magnetization plateaus induced by quantum interactions and an amplified magnetocaloric effect near magnetization shifts [49].

In our study, we focus on the $\text{Cu}_3 - X$ ($X = \text{As}, \text{Sb}$) configuration, characterized by its isosceles triangular structure. Earlier studies by Choi et al. [36, 38, 39] has shown that the behavior of this configuration is well-represented by the Heisenberg model, due to its triangular framework. Additionally, the study of the MCE in Cu_3 -like spin systems has been instrumental in elucidating their fundamental properties, especially in the low temperature region [52].

The structure of this paper is as follows: Sec. 2 introduces the thermodynamics of the model and outlines the quantum machines process. Sec. 3 delves into the Carnot machine, followed by an analysis of the Otto machine in Sec. 4. Similarly, in sec. 5 we discuss the Stirling engine. Finally, we conclude our findings and implications in Sec. 6.

II. THERMODYNAMICS OF THE MODEL

To investigate the quantum thermodynamics relevant for quantum machine applications, we consider energy levels of a spin Hamiltonian pertinent to Cu_3 -like systems, leveraging the Heisenberg model set within an isosceles triangular spin ring context [36, 38, 39]. This exploration, rooted in previous studies, focuses on a Hamiltonian that encapsulates the characteristics of Cu_3 compounds [36, 38, 39]. The Hamiltonian is mathemati-

Table I. Magnetic parameters of the $\{\text{Cu}_3 - X\}$ compounds adjusted to experimental data in units of Kelvin, where X denotes either As or Sb, as extracted from reference Magnetic[38].

Parameters	{Cu ₃ - As}	{Cu ₃ - Sb}
$J_{1,2}^x = J_{1,2}^y$	4.50 K	4.49 K
$J_{1,2}^z$	4.56 K	4.54 K
$J_{2,3}^x = J_{2,3}^y = J_{3,1}^x = J_{3,1}^y$	4.03 K	3.91 K
$J_{2,3}^z = J_{3,1}^z$	4.06 K	3.96 K
$D_{1,2}^z = D_{2,3}^z = D_{3,1}^z$	0.529 K	0.517 K
$D_{1,2}^x = D_{1,2}^y$	0.529 K	0.517 K
$g_1^x = g_1^y$	2.25	2.24
$g_2^x = g_2^y$	2.10	2.11
$g_3^x = g_3^y$	2.40	2.40
$g_1^z = g_2^z = g_3^z$	2.06	2.07

cally expressed as

$$\mathbf{H} = \sum_{j=1}^3 \sum_{\alpha=x,y,z} J_{j,j+1}^{\alpha} S_j^{\alpha} S_{j+1}^{\alpha} + \sum_{j=1}^3 \left[\mathbf{D}_{j,j+1} \cdot (\mathbf{S}_j \times \mathbf{S}_{j+1}) + \mu_B \mathbf{S}_j \cdot \mathbf{g}_j \cdot \mathbf{B}_j \right], \quad (1)$$

where $J_{j,j+1}^{\alpha}$ (simplified as J_j^{α}) represents the exchange interaction parameters between site j and $j+1$ for component $\alpha = \{x, y, z\}$. Whereas in second term $\mathbf{D}_{j,j+1}$ indicates the Dzyaloshinskii-Moriya interaction vector, denoted as $\mathbf{D}_{j,j+1} = (D_{j,j+1}^x, D_{j,j+1}^y, D_{j,j+1}^z)$. The site-dependent g -factors are defined as $\mathbf{g}_j = (g_j^x, g_j^y, g_j^z)$, while the last term corresponds to the magnetic field \mathbf{B} , which we assume to be independent of the spin site on the triangle. Here, μ_B denotes the Bohr magneton. The specific parameters were obtained using Electron Spin Resonance (ESR) data [36, 38, 39], and these parameters are reproduced in table I for both compounds. It is worth mentioning that only $\mathbf{D}_{1,2} = (D, D, D)$ is isotropic, while $\mathbf{D}_{2,3}$ and $\mathbf{D}_{3,1}$ contribute solely to the z -component, expressed as $\mathbf{D}_{2,3} = \mathbf{D}_{3,1} = (0, 0, D)$.

For convenience, the Hamiltonian (1) is expressed in Kelvin (K) units, redefining μ_B as $\hat{\mu}_B = \frac{\mu_B}{k_B} = 0.6717156644\text{K/T}$, where k_B denotes the Boltzmann constant, thereby simplifying the measurements of the magnetic field \mathbf{B} in Tesla (T) units. This conversion implies all subsequent units are in terms of k_B .

The eigenvalues of the Hamiltonian (1) are obtained through numerical diagonalization, essential for understanding the energy spectrum of the system under a fixed magnetic field.

Consequently, the partition function can symbolically be represented by

$$\mathcal{Z}(T, B) = \text{tr} \left(e^{-\mathbf{H}/T} \right) = \sum_{i=1}^8 e^{-\varepsilon_i(B)/T}, \quad (2)$$

where the eigenvalues $\varepsilon_i(B)$ depend on the Hamiltonian parameters provided in table I and the magnetic field \mathbf{B}

(in Tesla), with temperature T (in Kelvin) of the system. Any physical quantity can be derived from the partition function (2). However, as the eigenvalues can only be obtained numerically, analytical solution becomes restricted.

This result, tailored to the quantum machine context, emphasizes the significance of understanding magnetic and thermodynamic properties at a quantum level, crucial for advancing quantum machine technologies.

A. Internal energy, entropy, heat and work

Here we consider the Cu_3 -like compound, which has a finite number of energy levels given by eq.(1). In order to explore quantum machine, we need to express the average internal energy as follows:

$$U(T, B) = \sum_{i=1}^8 \varepsilon_i p_i. \quad (3)$$

here p_i is the distribution probability for i -th energy level, which depends implicitly of magnetic field B and temperature T , as well as ε_i depends implicitly of magnetic field B .

In quantum thermodynamics, the first law of thermodynamics is expressed as

$$dU = dQ + dW, \quad (4)$$

where $dQ = TdS$, with entropy given by

$$S(T, B) = -k_B \sum_{i=1}^8 p_i \ln(p_i), \quad (5)$$

Therefore, we can express dQ as

$$dQ = \sum_{i=1}^8 \varepsilon_i dp_i, \quad (6)$$

whereas dW becomes

$$dW = \sum_{i=1}^8 p_i d\varepsilon_i. \quad (7)$$

B. Quantum process

The work done is linked to changes in energy levels ε_i , aligning with the principle that work results from altering an external parameter, in this case, the magnetic field B .

Quantum isothermal process In a Cu_3 -like system, applying a magnetic field variation needs simultaneous adjustments in energy gaps and occupation probabilities to maintain equilibrium with the heat bath at every instant.

Table II. Characteristic of work and heat allowed by the second law of thermodynamics. The signal (+) means work done by the system and heat absorbed; (-) means work done on the system and heat released.

Operation mode	W_{net}	Q_{in}	Q_{out}	Thermal efficiency
Heat engine	+	+	-	$\eta = \frac{W_{net}}{Q_{in}}$
Refrigerator	-	-	+	$COP = \frac{Q_{in}}{W_{net}}$
Heater	-	-	-	$COP = \frac{Q_{out}}{W_{net}}$
Accelerator	-	+	-	$COP = \frac{Q_{out}}{W_{net}}$

Quantum isomagnetic process For a Cu_3 -like compound in contact with a heat bath, no work is performed during this process. Instead, heat transfer occurs between hot and cold temperatures. The occupation probabilities p_i and entropy \mathcal{S} evolve until the compound equilibrates thermally with the heat bath.

Quantum adiabatic process This process is characterized by constant population distributions ($dp_i = 0$), indicating no heat exchange ($dQ = 0$). However, work may still occur. Notably, the quantum adiabatic process is a specific case within the broader classical adiabatic framework[53].

C. Conditions for operational modes of a quantum machine

By adjusting the cycle parameters, one can invert the total work of cycle, aligning with the second law of thermodynamics. This law, especially in the context of different temperatures ($T_h > T_l$), helps define the operational regions for any thermodynamic cycle, as formulated by Clausius.

Heat engine The system absorbs heat from the hotter bath at T_h ($Q_{in} > 0$) and releases it into the cooler one at T_l ($Q_{out} < 0$). It partially converts the heat flow between these reservoirs into work ($W_{net} > 0$), with less external work needed for isothermal compression compared to work generated in isothermal expansion.

Refrigerator This mode induces heat flow from the cooler bath at T_l to the hotter one at T_h . Here, the Cu_3 -like compound absorbs heat from T_l ($Q_{out} > 0$) and releases it at T_h ($Q_{in} < 0$). The work input exceeds the work output ($W_{net} < 0$), inducing this heat transfer.

Accelerator Operates by utilizing work ($W_{net} < 0$) to enhance heat flow from the hotter bath at T_h to the cooler one at T_l ($Q_{in} > 0$ and $Q_{out} < 0$).

Heater Employs the work done ($W_{net} < 0$) to generate heat flow in both baths, leading to the working compound releasing heat in both ($Q_{in} < 0$ and $Q_{out} < 0$).

D. Thermal efficiency

In the heat engine mode, the efficiency of quantum engine, as shown in Table II, with $\eta < 1$. The coefficient of

performance (COP) for other operation modes is also detailed in Table II. Given that COPs are typically greater than one, we introduce an alternative expression

$$\kappa = \frac{COP}{1 + COP}. \quad (8)$$

This new metric evaluates COP within a bounded range of $0 < \kappa < 1$, implying that as COP approaches 0, κ similarly trends toward 0, while κ approaches 1 as COP tends to infinity. Additionally, a $COP = 1$ corresponds to $\kappa = 0.5$. Consequently, the thermal efficiency for all operational modes can be defined within the range of 0 to 1, with 0 indicating the worst performance and 1 the best. This definition is applicable for the refrigerator, heater, and accelerator, each described in Table II.

For our discussion, we will focus on the $\text{Cu}_3 - \text{As}$ compound. The $\text{Cu}_3 - \text{Sb}$ compound demonstrates similar characteristics, as shown by the comparable parameters in Table I.

III. QUANTUM CARNOT MACHINE

The quantum Carnot machine is a theoretical concept showing the highest efficiency possible for a heat engine. It's key for understanding how efficiently energy can be used in quantum systems like the Cu_3 -like compound. This idea is really useful in the field of quantum thermodynamics, helping us learn about how energy works at the quantum level.

According to Fig.1, we will describe all the steps of the Carnot cycle below. For simplicity, we will assume, without losing generality, that when the external magnetic field is increased, the spins try to align parallel to the external magnetic field. Although this is not the general rule, frustration can invert this process (see [52]). However, our analysis will still remain the same; the only change would be that instead of heat being observed, heat will be released or vice versa.

1. Isothermal magnetization process (a-b): The Cu_3 -like compound is placed in a isolated environment. When it comes into contact with a colder reservoir at temperature T_l , the external magnetic field gradually increases, causing the Cu_3 -like compound to release heat to the cold reservoir,

$$Q_{ab} = T_l [\mathcal{S}(T_l, B_b) - \mathcal{S}(T_l, B_0)], \quad (9)$$

decreasing magnetic entropy and aligning the spins with the magnetic field. According to the quantum adiabatic condition $p_i(T_l, B_b) = p_i(T_h, B_1)$, which implies that $\mathcal{S}(T_l, B_b) = \mathcal{S}(T_h, B_1)$, thus we have

$$Q_{ab} = T_l [\mathcal{S}(T_h, B_1) - \mathcal{S}(T_l, B_0)]. \quad (10)$$

The change in internal energy in the isothermal process at low temperature T_l is

$$\Delta U_{ab} = U(T_l, B_b) - U(T_l, B_0), \quad (11)$$

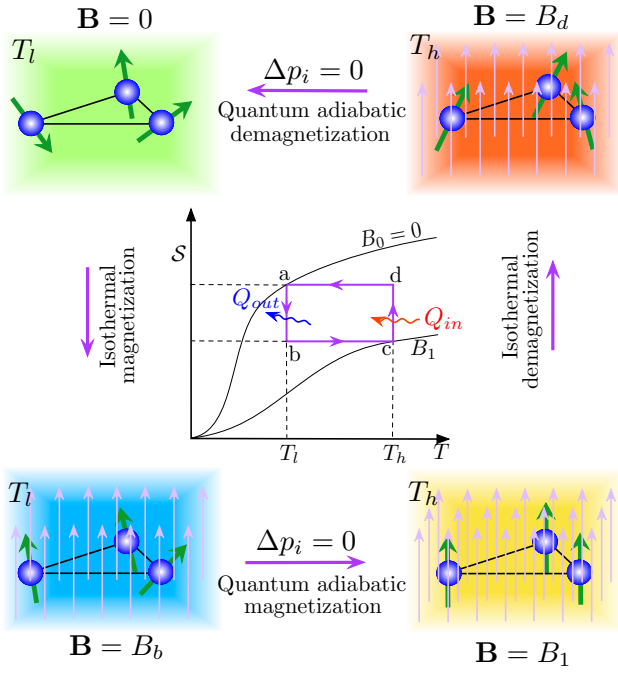


Figure 1. Schematic representation of Quantum Carnot machine cycle for Cu_3 -like compound. Magnetic field is turned on (B_1) or turned off ($B_0 = 0$).

and the corresponding work done is

$$W_{ab} = Q_{ab} - \Delta U_{ab}. \quad (12)$$

2. Adiabatic magnetization process (b-c): The system is again isolated, and the magnetic field is increased to B_1 aligning the spins. Since this process is a quantum adiabatic $Q_{bc} = 0$, and the temperature of the system rises to T_h . Therefore, the variation energy becomes

$$\Delta U_{bc} = U(T_h, B_1) - U(T_l, B_b), \quad (13)$$

and the respective work done is

$$W_{bc} = -\Delta U_{bc} = U(T_l, B_b) - U(T_h, B_1),$$

$$= \sum_{i=1}^8 [\varepsilon_i(B_b) p_i(T_l, B_b) - \varepsilon_i(B_1) p_i(T_h, B_1)], \quad (14)$$

using the quantum adiabatic condition $p_i(T_l, B_b) = p_i(T_h, B_1)$ the work done will become

$$W_{bc} = \sum_{i=1}^8 [\varepsilon_i(B_b) - \varepsilon_i(B_1)] p_i(T_h, B_1), \quad (15)$$

3. Isothermal demagnetization process (c-d). The system is brought into thermal contact with a hot reservoir at temperature T_h . The external magnetic field is gradually decreased. During this process, the Cu_3 -like absorb heat from the reservoir

$$Q_{cd} = T_h [\mathcal{S}(T_h, B_d) - \mathcal{S}(T_h, B_1)], \quad (16)$$

and their spin orientations become more disordered, increasing the magnetic entropy. Since the quantum adiabatic condition $p_i(T_h, B_d) = p_i(T_l, B_0)$, which implies that $\mathcal{S}(T_h, B_d) = \mathcal{S}(T_l, B_0)$, thus we have

$$Q_{cd} = T_h [\mathcal{S}(T_l, B_0) - \mathcal{S}(T_h, B_1)]. \quad (17)$$

The variation of internal energy at hot bath with temperature T_h is

$$\Delta U_{cd} = U(T_h, B_d) - U(T_h, B_1) \quad (18)$$

The corresponding work done is

$$W_{cd} = Q_{cd} - \Delta U_{cd}. \quad (19)$$

4. Adiabatic demagnetization process (d-a). The system is isolated from any heat reservoir, and the external magnetic field is further decreased. This process is adiabatic and the temperature of the system drops to T_l without any heat exchange $Q_{da} = 0$. And corresponding variation energy becomes

$$\Delta U_{da} = U(T_l, B_0) - U(T_h, B_d), \quad (20)$$

the work done is

$$W_{da} = -\Delta U_{da} = U(T_h, B_d) - U(T_l, B_0),$$

$$= \sum_{i=1}^8 [\varepsilon_i(B_d) p_i(T_h, B_d) - \varepsilon_i(B_0) p_i(T_l, B_0)], \quad (21)$$

using the quantum adiabatic condition $p_i(T_h, B_d) = p_i(T_l, B_0)$ the work done results in

$$W_{da} = \sum_{i=1}^8 [\varepsilon_i(B_1) - \varepsilon_i(B_d)] p_i(T_l, B_0), \quad (22)$$

Finally, the net work is given by

$$W_{net} = W_{ab} + W_{bc} + W_{cd} + W_{da} \quad (23)$$

or equivalently

$$W_{net} = Q_{ab} + Q_{cd}.$$

The heat absorbed and released are respectively $Q_{in} = Q_{ab}$ and $Q_{out} = Q_{cd}$.

Certainly, it is essential to consider the heat engine efficiency, denoted as η give by $\eta = 1 + Q_{out}/Q_{in} = 1 - T_l/T_h$. When the Carnot engine operates as a refrigerator, the COP becomes $COP = Q_{in}/W_{net} = \frac{T_h}{T_h - T_l}$. Obviously, for the Carnot engine, both thermal efficiencies are unaffected by the magnetic field.

In Fig. 2, we depict the operational modes of the quantum Carnot cycle for a Cu_3 -like compound in the B_0 versus B_1 plane. The green region represents the heat

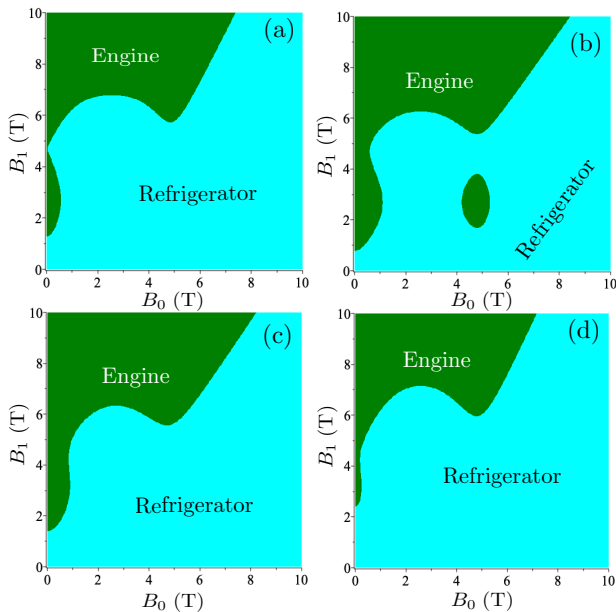


Figure 2. Operational modes of the quantum Carnot cycle for Cu_3 -like compound in the B_0 - B_1 plane. The green region operates as engine, while the cyan region operates as refrigerator. (a) For $T_l = 0.5\text{K}$ and $T_h = 1\text{K}$. (b) For $T_l = 0.7\text{K}$ and $T_h = 1\text{K}$. (c) For $T_l = 0.7\text{K}$ and $T_h = 1.5\text{K}$. (d) For $T_l = 1\text{K}$ and $T_h = 1.5\text{K}$.

engine mode, while the cyan region denotes the refrigerator mode. The cycle is evaluated under varying cold (T_l) and hot (T_h) temperature conditions. In panel (a), we illustrate the scenario with $T_l = 0.5\text{K}$ and $T_h = 1\text{K}$. To explore the MCE, we assume $B_0 = 0$. We observe that for B_1 greater than approximately 1.2, the system operates as a heat engine. However, with a non-null B_0 , the system could function as a refrigerator at B_1 around 4.7T, where the MCE exhibits better enhancement [52]. In this case, the heat engine efficiency remains constant within the entire green region at $\eta = 0.5$, while the COP for the refrigerator is $COP = 2$. In panel (b), with $T_l = 0.7\text{K}$ and $T_h = 1\text{K}$, we observe a similar behavior. The Cu_3 -like compound could work as a refrigerator at B_1 around 4.7T improved by the MCE[52]. However, a small region also appears as a heat engine at B_0 around 5T and B_1 around 3T. In this scenario, the heat engine efficiency remains constant within the green region at $\eta = 0.3$, while the COP for the refrigerator is $COP = 3.333$. Moving to panel (c) with $T_l = 0.7\text{K}$ and $T_h = 1.5\text{K}$, the region where the system operates as a heat engine for B_0 around 5T and B_1 around 3T disappears. However, the system continues to operate as a heat engine for B_0 around 0T and B_1 around 4.7T. The heat engine efficiency remains constant within the green region at $\eta = 0.533$, while the COP for the refrigerator is $COP = 1.875$. Finally, in panel (d) with $T_l = 1\text{K}$ and $T_h = 1.5\text{K}$, the behavior is quite similar to panel (a), although for $B_0 = 0$ and B_1 greater than approximately 2.5T, it operates as a heat engine. In this case, the heat engine efficiency is $\eta = 0.333$

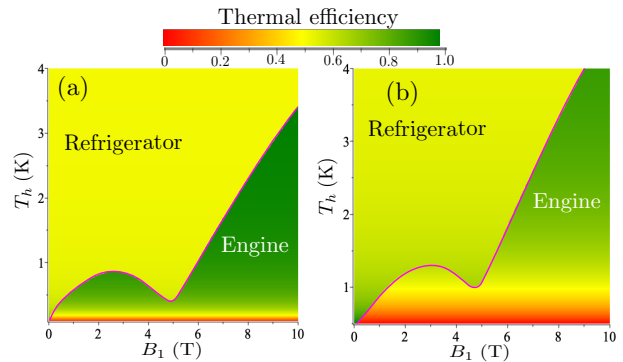


Figure 3. Operational modes of the quantum Carnot cycle for Cu_3 -like compound in the B_1 - T_h plane. Below the pink curve operates as a heat engine, while above the curve operates as a refrigerator. (a) For $T_l = 0.1\text{K}$ and $B_0 = 0\text{T}$. (b) For $T_l = 0.5\text{K}$ and $B_0 = 0\text{T}$.

within the green region, while the COP for the refrigerator is $COP = 3$.

Another interesting analysis would involve examining the operational mode in the $B_0 - T_h$ plane, as illustrated in Fig.3. In Panel (a), we consider $T_l = 0.1\text{K}$ and $B_0 = 0$. The pink curve serves as the boundary between the two operational modes: heat engine and refrigerator. Whereas in panel (c), we present a density plot that indicates the thermal efficiency under the same conditions as in panel (a). Here, we observe that the refrigerator operation COP is consistently above 1, or equivalently, κ is greater than approximately 0.5. Meanwhile, the efficiency of the Carnot heat engine remains roughly above 0.8 in a vast region. As we increase the temperature T_h , the system becomes more efficient, leading roughly $\eta \approx 0.96$. Panel (b) shows a similar plot but assumes a fixed $T_l = 0.5\text{K}$ and $B_0 = 0$. Once again, the pink curve delineates the boundary between the heat engine and refrigerator operation modes. Essentially, we observe a similar behavior here, although the COP of the refrigerator consistently exceeds 1, or κ is approximately 0.6. Meanwhile, the efficiency of the heat engine at low T_h is inferior, and for higher temperatures, η becomes more efficient but remains lower than in panel (a). It is worth noting that for each operational mode, the thermal efficiency remains independent of the magnetic field B_1 .

Hence, comprehending the quantum Carnot engine of Cu_3 -like compounds is a crucial step in exploring quantum phenomena for practical technological progress.

IV. QUANTUM OTTO MACHINE

Now we will look at how a compound similar to Cu_3 could work as a quantum Otto machine. This study is important for the field of quantum thermodynamics, as it offers insights into how Cu_3 -like quantum systems might be used for energy conversion. Understanding the quantum versions of classical thermodynamic processes can

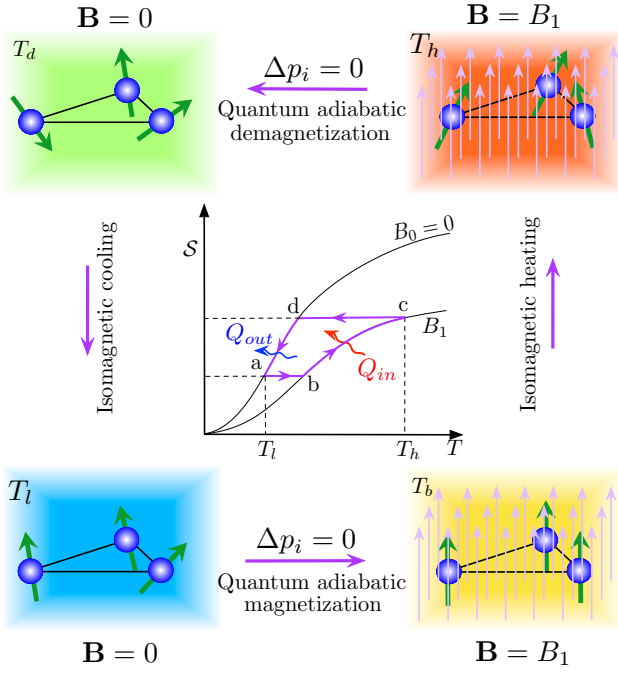


Figure 4. Schematic representation of Quantum Otto machine cycle for a Cu_3 -like compound. Magnetic field is turned on or turned off.

help us better manage energy at a tiny, microscopic scale.

1. Adiabatic magnetization process (a-b): In this process, the system isolates itself from the reservoir. The external magnetic field increases from B_0 to B_1 , aligning the spin orientation. No heat is transferred ($Q_{ab} = 0$), even as the temperature rises. Consequently, the change in energy is

$$\Delta U_{ab} = U(T_b, B_1) - U(T_l, B_0) \quad (24)$$

and the work done is

$$W_{ab} = -\Delta U_{ab} = U(T_l, B_0) - U(T_b, B_1), \\ = \sum_{i=1}^8 [\varepsilon_i(B_0)p_i(T_l, B_0) - \varepsilon_i(B_1)p_i(T_b, B_1)], \quad (25)$$

using the quantum adiabatic condition $p_i(T_b, B_1) = p_i(T_l, B_0)$, we can obtain

$$W_{ab} = \sum_{i=1}^8 [\varepsilon_i(B_0) - \varepsilon_i(B_1)] p_i(T_l, B_0). \quad (26)$$

2. Isomagnetic process (b-c): In this stage, the system comes into thermal contact with a hot reservoir, and the temperature increases while keeping the magnetic field constant. No work is done, $W_{bc} = 0$. Consequently, the system absorbs heat, which is

given by

$$Q_{bc} = \Delta U_{bc} = U(T_h, B_1) - U(T_b, B_1), \\ = \sum_{i=1}^8 \varepsilon_i(B_1) [p_i(T_h, B_1) - p_i(T_b, B_1)]. \quad (27)$$

Taking into account the quantum adiabatic condition, $p_i(T_b, B_1) = p_i(T_l, B_0)$, thus the heat becomes

$$Q_{bc} = \sum_{i=1}^8 \varepsilon_i(B_1) [p_i(T_h, B_1) - p_i(T_l, B_0)]. \quad (28)$$

3. Adiabatic demagnetization process (c-d): In this stage, the Cu_3 -like system is once again isolated from the reservoir, and the external magnetic field decreases adiabatically ($Q_{cd} = 0$), causing the system to cool. The corresponding change energy reads

$$\Delta U_{cd} = U(T_d, B_0) - U(T_h, B_1), \quad (29)$$

and the work done is .

$$W_{bc} = -\Delta U_{bc} = U(T_h, B_1) - U(T_d, B_0), \\ = \sum_{i=1}^8 [\varepsilon_i(B_1)p_i(T_h, B_1) - \varepsilon_i(B_0)p_i(T_d, B_0)]. \quad (30)$$

considering the quantum adiabatic condition where $p_i(T_d, B_0) = p_i(T_h, B_1)$, we have

$$W_{bc} = \sum_{i=1}^8 [\varepsilon_i(B_1) - \varepsilon_i(B_0)] p_i(T_h, B_1). \quad (31)$$

4. Isomagnetic process (d-a): In this process, the system comes into contact with a cold environment, gradually lowering its temperature. Since there is no change in the magnetic field, no work is done ($W_{da} = 0$). The heat released to the environment is given by

$$Q_{da} = \Delta U_{da} = U(T_l, B_0) - U(T_d, B_0), \\ = \sum_{i=1}^8 \varepsilon_i(B_0) [p_i(T_l, B_0) - p_i(T_d, B_0)]. \quad (32)$$

Considering the quantum adiabatic condition given by $p_i(T_d, B_0) = p_i(T_h, B_1)$, we obtain

$$Q_{cd} = \sum_{i=1}^8 \varepsilon_i(B_0) [p_i(T_l, B_0) - p_i(T_h, B_1)]. \quad (33)$$

Finally, the total work done is given by

$$W_{net} = \sum_{i=1}^8 [\varepsilon_i(B_1) - \varepsilon_i(B_0)] [p_i(T_h, B_1) - p_i(T_l, B_0)]. \quad (34)$$

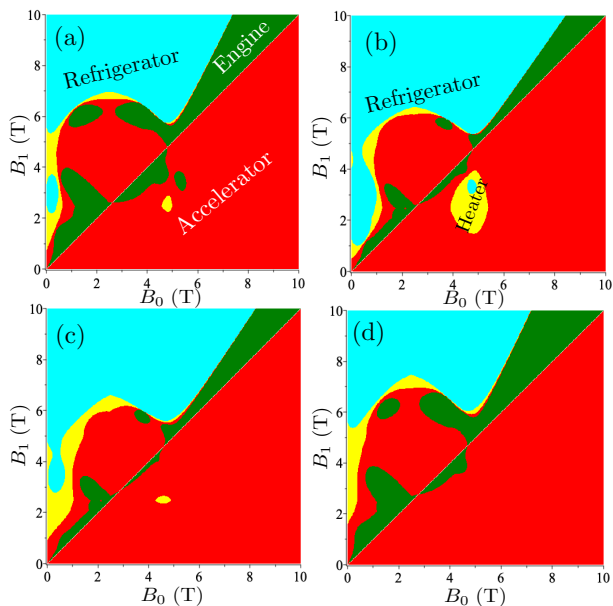


Figure 5. Operational modes of the quantum Otto cycle for Cu_3 -like compound in the $B_0 - B_1$ plane. In green region operates as engine, in cyan region operates as refrigerator, the yellow region operates as heater, and in red region operates accelerator. (a) For $T_l = 0.5\text{K}$ and $T_h = 1\text{K}$. (b) For $T_l = 0.7\text{K}$ and $T_h = 1\text{K}$. (c) For $T_l = 0.7\text{K}$ and $T_h = 1.5\text{K}$. (d) For $T_l = 1\text{K}$ and $T_h = 1.5\text{K}$.

In Fig. 5, we present the operational modes of the quantum Otto cycle for a Cu_3 -like compound in the $B_0 - B_1$ plane. The color-coded regions signify different modes of operation: the green region represents the engine mode, the cyan region represents the refrigerator mode, the yellow region corresponds to the heater mode, and the red region indicates the accelerator mode. In Panel (a), we consider the case with $T_l = 0.5\text{K}$ and $T_h = 1\text{K}$. Just to explore the MCE, we assume conveniently B_0 is approximately 0.1T . Notably, the system exhibits peculiar behavior in the range of $2.2\text{T} \lesssim B_1 \lesssim 3.8\text{T}$, where it functions as a refrigerator. However, at $B_1 \approx 4\text{T}$, where the MCE is significantly enhanced, the system operates as a thermal accelerator. For $B_0 > B_1$, the system predominantly acts as a thermal accelerator, while for $B_1 > B_0$, it exhibits four operation modes. Specifically, for $B_1 \gtrsim B_0$, the system serves as a heat engine, and where the MCE is enhanced, it behaves as an accelerator. In Panel (b), with $T_l = 0.7\text{K}$ and $T_h = 1\text{K}$, we observe similar behavior. Although in this case, the Cu_3 -like compound could work as a refrigerator at $B_1 \approx 1\text{T}$. However, a small region appears as a refrigerator at $B_0 \approx 5\text{T}$, surrounded by a heater operation mode. In Panel (c), for $T_l = 0.7\text{K}$ and $T_h = 1.5\text{K}$, the region where the system operates as a refrigerator and heater at $B_0 \approx 5\text{T}$ and $B_1 \approx 3\text{T}$ disappears. However, for $B_0 \approx 0.1\text{T}$ and $B_1 \approx 3\text{T}$, the system continues to operate as a refrigerator. Similarly, in Panel (d), for $T_l = 1\text{K}$ and $T_h = 1.5\text{K}$, the behavior is somewhat akin to panel (a), although for

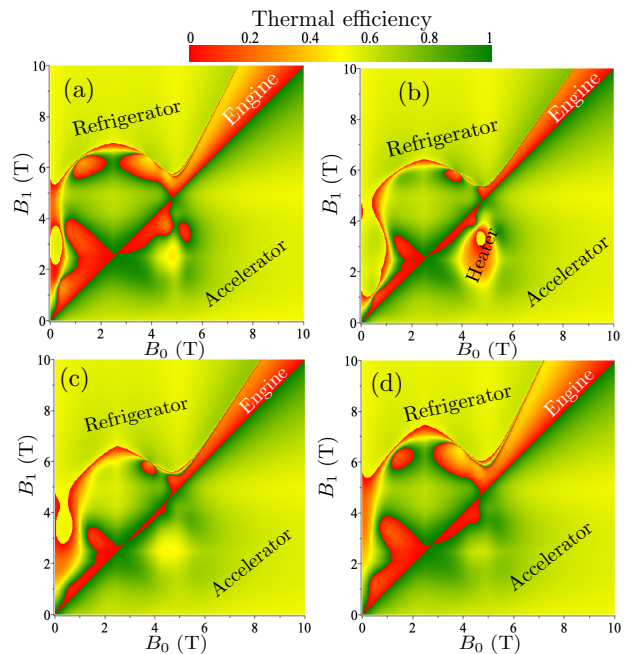


Figure 6. Thermal efficiency of the quantum Otto cycle for Cu_3 -like compound in the $B_0 - B_1$ plane. The cycle is evaluated under varying cold (T_l) and hot (T_h) temperature conditions: (a) For $T_l = 0.5$ and $T_h = 1$. (b) For $T_l = 0.7$ and $T_h = 1$. (c) For $T_l = 0.7$ and $T_h = 1.5$. (d) For $T_l = 1$ and $T_h = 1.5$.

$B_0 = 0$ and $B_1 \gtrsim 5\text{T}$, it operates as a refrigerator.

In contrast to the Carnot engine discussed in the previous section, the Otto engine can operate in four distinct modes: heat engine, refrigerator, heater, and accelerator.

For engine heat, we use η to represent thermal efficiencies, while for different COPs for the refrigerator, heater, and accelerator, we employ the eq. (8). This information is presented in Fig.6, using the same parameter set as in Fig.2. In this representation, regions shaded in red indicate poor efficiency, green regions correspond to the best efficiency, and yellow regions indicate efficiency values of $\eta = 0.5$. Similarly, for COPs, $\kappa = 0.5$ corresponds to $COP = 1$. Broadly, we observe that $\kappa \gtrsim 0.5$ or $COP \gtrsim 1$, while for heat engines, $\eta \lesssim 0.5$. This essentially means that no heat engine achieves an efficiency greater than $\eta > 0.5$.

Additionally, we can analyze the quantum operational modes as functions of the hot temperature T_h and magnetic field B_1 , assuming $B_0 = 0\text{T}$. In contrast to the Carnot engine, thermal efficiency now depends on the magnetic fields B_0 and B_1 , as well as the temperatures T_l and T_h . In Fig.7, Panel (a) illustrates the operational modes of the quantum Otto cycle for a Cu_3 -like compound in the $B_1 - T_h$ plane, assuming fixed values of $T_l = 0.1\text{K}$ and $B_0 = 0$. Under these conditions, we observe all four operational modes: engine (green), refrigerator (cyan), heater (yellow), and accelerator (red). Panel (b) presents a similar plot but assumes $T_l = 0.5\text{K}$ and $B_0 = 0\text{T}$. It demonstrates that at lower temperatures,

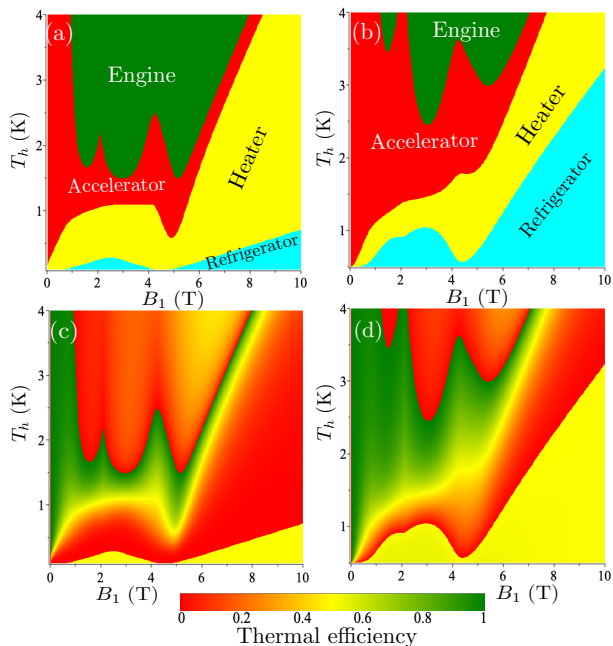


Figure 7. (a) Operation mode of the quantum Otto cycle for Cu_3 -like compound in the plane $B_1 - T_h$, for $T_l = 0.1$ and $B_0 = 0$. (b) For $T_l = 0.5$ and $B_0 = 0$. (c-d) Thermal efficiency under the same condition to (a-b) respectively.

the system can function as a refrigerator, although this region significantly decreases for lower T_h values. Conversely, for higher temperatures, the system tends to operate as a heat engine. In panels (c-d), we depict the thermal efficiency under the same conditions as in panels (a-b), respectively. For thermal efficiency, we use η for the heat engine and κ for the refrigerator, heater, and accelerator, as detailed in Table II. Here, we can observe that thermal efficiency depends on T_h and B_1 . The COP of the refrigerator is roughly around $COP = 1$ or $\kappa = 0.5$, while the efficiency of the heat engine is approximately $\eta \sim 0.2$. The COP for the heater is also quite small. However, the efficiency of the thermal accelerator is notably strong, approaching $\kappa \rightarrow 1$.

Hence, the Cu_3 -like compound may offer certain advantages, mainly in low-temperature region around MCE is relevant, around $B_1 \sim 4.7\text{T}$, and for temperature $T_h \gtrsim 2\text{K}$, the heat engine operates with high efficiency roughly around $\eta \sim 0.5$.

As technology increasingly miniaturizes and ventures into the quantum domain, insights from the quantum Otto engine could lead to the development of highly efficient, novel quantum technologies and devices, with wide-ranging applications from computing to material science.

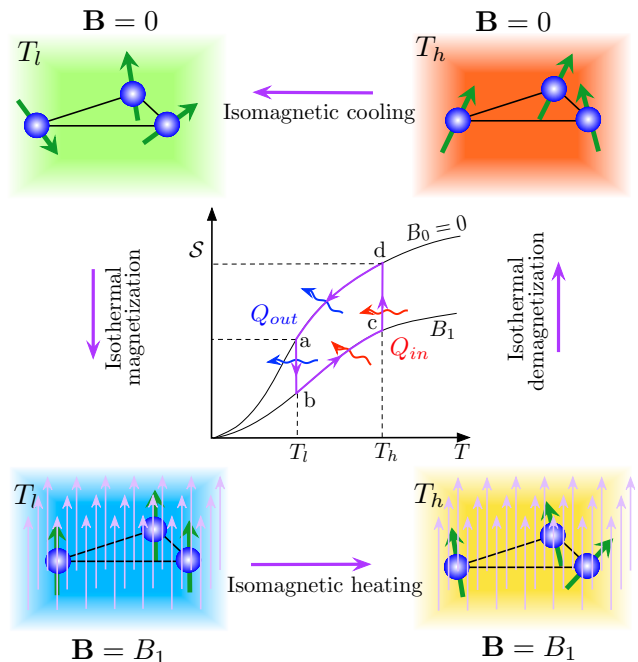


Figure 8. Schematic representation of Quantum Stirling machine cycle for a Cu_3 -like compound. Magnetic field is turned on or turned off.

V. QUANTUM STIRLING MACHINE

Finally, we consider how Cu_3 -like compound could work as a quantum Stirling machine which represents a relevant stride in the field of quantum thermodynamics, offering insights into the manipulation and potential applicability of quantum Cu_3 -like systems for energy conversion. By understanding the quantum mechanical counterparts of classical thermodynamic processes, could help the energy management at microscopic scales.

1. Isothermal magnetization process (a-b). In this process the temperature is hold constant T_l , and increases gradually the magnetic field up to B_1 , consequently the magnetic entropy decreases. The internal energy variation is given by

$$\Delta U_{ab} = U(T_l, B_1) - U(T_l, B_0), \quad (35)$$

and the heat released to environment is

$$Q_{ab} = T_l [S(T_l, B_1) - S(T_l, B_0)]. \quad (36)$$

Therefore, the Cu_3 -like system work realized in this process becomes

$$W_{ab} = Q_{ab} - \Delta U_{ab}. \quad (37)$$

2. Isomagnetic process (b-c). In this process no work is realized by the compound, because the magnetic field holds constant $W_{bc} = 0$. However, the temperature of the system increases to T_h increasing the

magnetic entropy and spins alignments becoming more erratic, consequently the system absorb heat from the reservoir, which is given by

$$Q_{bc} = \Delta U_{bc} = U(T_h, B_1) - U(T_l, B_1),$$

$$= \sum_{i=1}^8 \varepsilon_i(B_1) [p_i(T_h, B_1) - p_i(T_l, B_1)]. \quad (38)$$

3. Isothermal process (c-d). In this process again the temperature remains constant at T_h , while external magnetic field is decreased absorbing heat from the reservoir

$$Q_{cd} = T_h [\mathcal{S}(T_h, B_0) - \mathcal{S}(T_h, B_1)], \quad (39)$$

when magnetic field is decreased the spin alignment start disarranging, leading to higher entropy. Therefore, the work realized in this process becomes

$$W_{cd} = Q_{cd} - \Delta U_{cd}. \quad (40)$$

The variation of internal energy at hot bath with temperature T_h is

$$\Delta U_{cd} = U(T_h, B_0) - U(T_h, B_1). \quad (41)$$

4. Isomagnetic process (d-a). Here the Cu₃-like system is placed in contact with cold bath consequently decreasing the magnetic entropy and then the temperature of the system also decreases, but since there is no change of magnetic field, then no work is realized $W_{da} = 0$. Thus the heat released to the cold bath by the system is given by

$$Q_{da} = \Delta U_{da} = U(T_l, B_0) - U(T_h, B_0),$$

$$= \sum_{i=1}^8 \varepsilon_i(B_0) [p_i(T_l, B_0) - p_i(T_h, B_0)]. \quad (42)$$

The total work done can be expressed as a sum of the all works done

$$W_{net} = W_{ab} + W_{cd}, \quad (43)$$

whereas the heat absorbed by the system becomes

$$Q_{in} = Q_{bc} + Q_{cd} \quad (44)$$

and the heat released to the cold bath is

$$Q_{out} = Q_{da} + Q_{ab}. \quad (45)$$

In Fig.9, we present the quantum operational modes of the Stirling cycle for an engine using a Cu₃-like compound in the $B_0 - B_1$ plane. Panel (a) illustrates this for fixed temperatures $T_l = 0.5\text{K}$ and $T_h = 1\text{K}$. It is clear

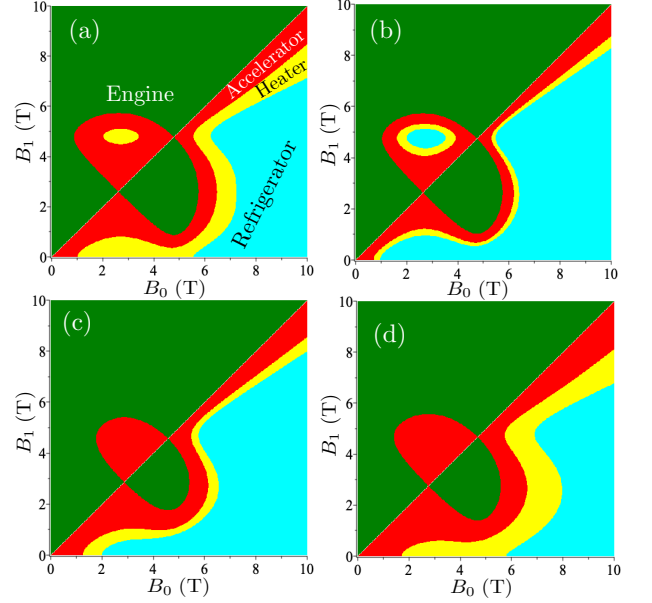


Figure 9. Operational modes of the quantum Stirling cycle for Cu₃-like compound in the B_0 - B_1 plane. In green region operates as engine, in cyan region operates as refrigerator, the yellow region operates as heater, and in red region operates as accelerator. (a) For $T_l = 0.5\text{K}$ and $T_h = 1\text{K}$. (b) For $T_l = 0.7\text{K}$ and $T_h = 1\text{K}$. (c) For $T_l = 0.7\text{K}$ and $T_h = 1.5\text{K}$. (d) For $T_l = 1\text{K}$ and $T_h = 1.5\text{K}$.

that when $B_1 > B_0$, the system mainly operates as a heat engine. Conversely, when $B_1 < B_0$, the system functions as a refrigerator. Interestingly, around $B_0 \sim 4.5\text{T}$ and $B_1 \sim 3\text{T}$, there is a region where it operates as a heat engine. In contrast, around $B_0 \sim 3\text{T}$ and $B_1 \sim 4.5\text{T}$, the system functions as an accelerator. There is even a small region at $B_0 \sim 3\text{T}$ and $B_1 \sim 5\text{T}$ where it operates as a heater. Additionally, between these two main operational modes, there are regions where the heater and thermal accelerator modes occur, particularly when $B_1 \lesssim B_0$. Panel (b) depicts the scenario for $T_l = 0.7\text{K}$ and $T_h = 1\text{K}$, showing a similar pattern to panel (a). The main difference is that the heater operation mode is significantly reduced. However, at $B_0 \sim 3\text{T}$ and $B_1 \sim 5$, the system operates as a refrigerator, surrounded by the heater operation mode. Moreover, for $B_0 \sim 4.5\text{T}$ and $B_1 \lesssim 1\text{T}$, the system acts as a refrigerator. In Panel (c), we plot the results for $T_l = 0.7\text{K}$ and $T_h = 1.5\text{K}$, which is again similar to (b). However, there are no heater or refrigerator modes at $B_0 \sim 3\text{T}$ and $B_1 \sim 5$, though the accelerator mode still remains at $B_0 \sim 4.5\text{T}$ and $B_1 \lesssim 1\text{T}$. Finally, Panel (d) presents results for a different set of parameters, $T_l = 1\text{K}$ and $T_h = 1.5\text{K}$. Here, we observe wider regions for the heater and accelerator modes, but the inversion operation mode still occurs at $B_0 \sim 3\text{T}$ and $B_1 \sim 4.5\text{T}$, and vice versa.

Our next analysis focuses on the thermal efficiency of the operating modes of the quantum Stirling engine. To conveniently present this, we display it in Fig.10, assum-

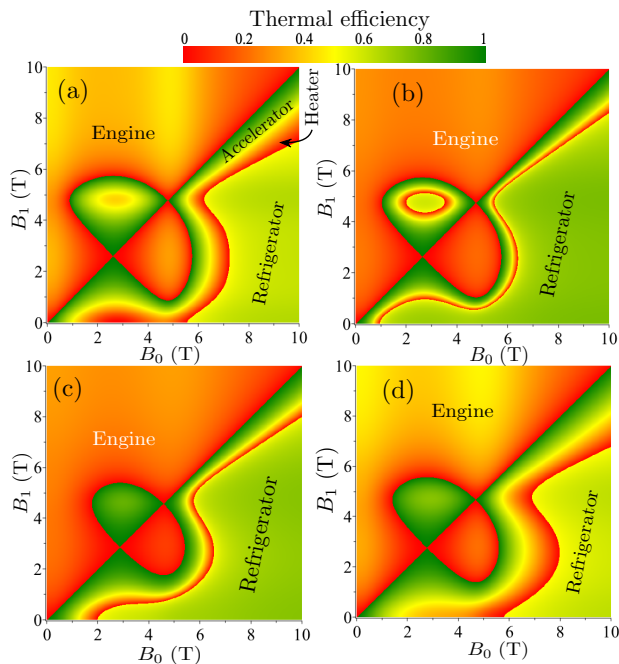


Figure 10. Thermal efficiency of the quantum Stirling cycle for Cu_3 -like compound in the B_0 - B_1 plane. The cycle is evaluated under varying cold (T_l) and hot (T_h) temperature conditions: (a) For $T_l = 0.5$ and $T_h = 1$. (b) For $T_l = 0.7$ and $T_h = 1$. (c) For $T_l = 0.7$ and $T_h = 1.5$. (d) For $T_l = 1$ and $T_h = 1.5$.

ing the conditions considered in Fig.9. We calculate the thermal efficiency using the values provided in Table II and Eq.(8). When the Stirling machine operates as a heat engine, the efficiency is notably $\eta \lesssim 0.5$ in the vast region where it functions. This efficiency is even higher in panel (a) for $B_1 \gtrsim 5\text{T}$ and when $B_1 > B_0$. On the other hand, when it operates as a refrigerator, the thermal efficiency is slightly above $\kappa \gtrsim 0.5$ or $COP \gtrsim 1$, showing better efficiency in panels (b-c). When the system works as a heater, the thermal efficiency is clearly below $\kappa < 0.5$ in most of the region where it operates. Finally, when the system functions as a thermal accelerator, the corresponding efficiency becomes considerably high.

It is worth noting that in the region where the magnetocaloric effect is more prominent, the quantum operation mode undergoes a type of inversion. Similar to the Otto machine, the Stirling machine has four operational modes: heat engine, refrigerator, heater, and accelerator. This exploration is not only academically intriguing but also holds potential practical applications. The quantum Stirling engine could serve as a prototype for elucidating the fundamental principles of quantum heat engines and potential technological application[54].

VI. CONCLUSIONS

This paper presents a theoretical investigation of the $\text{Cu}_3 - X$ ($X = \text{As}, \text{Sb}$) antiferromagnetic spin system, which is characterized by its slightly distorted equilateral triangular configuration. By employing the Heisenberg model on a triangular lattice, this study incorporates factors such as exchange interactions, Dzyaloshinskii-Moriya interaction, g-factors, and external magnetic fields to accurately represent the system properties, as emphasized in prior research[36, 38, 39]. The significance of the Cu_3 -like system has increased recently due to its fundamental properties and the potential for applications in emerging fields such as spintronics, nanotechnology, and biomedicine. This interest is driven by the diverse capabilities of several magnetic compounds. Additional analysis on the thermodynamics of the model, as discussed in earlier literature[52], reveals insights into the energy levels and thermodynamic behaviors under varying conditions of magnetic fields and temperatures. A particular focus was placed on the magnetocaloric effect (MCE) observed in $\text{Cu}_3 - X$, which is significantly prominent at low temperatures (around $T \approx 1\text{K}$) for perpendicular magnetic fields of approximately $\sim 5\text{T}$.

The implications of the MCE for the operation and efficiency of quantum machines have drawn considerable attention. Consequently, we explored the operational capabilities of three distinct quantum machines: the Carnot, Otto, and Stirling machines, within the context of a Cu_3 -like system. We highlight the influence of external magnetic fields and temperature on their performance. The Carnot machine shows dependence on the external magnetic field, demonstrating its capacity to operate as a heat engine for $B_1 \lesssim B_0$ and as a refrigerator for $B_1 \gtrsim B_0$. However, a notable shift in operational mode occurs near the MCE becomes more prominent, implying that the system functions as a heat engine even for $B_1 \gtrsim B_0$. In a similar vein, the quantum Otto machine displays versatility, functioning as a heat engine, refrigerator, heater, and thermal accelerator. It is primarily dominated by the thermal accelerator mode for $B_1 < B_0$, while it mainly serves as a refrigerator for $B_1 > B_0$. Nonetheless, there exists a small region for $B_1 \gtrsim B_0$ where it operates as a heat engine. The quantum Stirling machine, likewise, is capable of operating as a heat engine, thermal accelerator, heater, and refrigerator. It primarily functions as a heat engine for $B_1 > B_0$, while it acts mainly as a refrigerator for $B_1 < B_0$. Near the MCE, it alternates its operation between a heat engine and thermal accelerator, underscoring the MCE significance. We also examined the corresponding thermal efficiencies for all these engines.

Through this theoretical exploration, we aim to enhance the understanding of quantum heat machines and their technological applications, especially in low-temperature regimes where the MCE plays a pivotal role. Our findings highlight the adaptability and efficiency of these engines across various operational modes,

contributing valuable insights into the potential practical applications of the $\text{Cu}_3 - X$ antiferromagnetic spin system and similar compounds in the field of quantum thermodynamics.

ACKNOWLEDGMENTS

O. R. and M. Rojas thanks CNPq and FAPEMIG for partial financial support. M. Rojas acknowledges FAPEMIG Grant APQ-02226-22.

-
- [1] H. T. Quan, Y. X. Liu, C. P. Sun, F. Nori, *Phys. Rev. E*, **76**, 031105 (2007).
- [2] N. M. Myers, O. Abah, S. Deffner, *AVS Quantum Sci.* **4**, 027101 (2022).
- [3] R. Kosloff, *J. Chem. Phys.* **80**, 1625 (1984).
- [4] R. Alicki, *J. Phys. A: Math. Gen.* **12**, L103 (1979).
- [5] T. Zhang, W.-T. Liu, P.-X. Chen, Ch.-Z. Li, *Phys. Rev. A* **75**, 062102 (2007).
- [6] X. He, J. H. J. Zheng, *Physica A* **391**, 6594 (2012).
- [7] R. Kosloff, A. Levy, *Ann. Rev. Phys. Chem.* **65**, 365 (2014).
- [8] A. Insinga, B. Andresen, P. Salamon, *Phys. Rev. E* **94**, 012119 (2016).
- [9] Y. Rezek, R. Kosloff, *New J. Phys.* **8**, 83 (2006).
- [10] M. Josefsson, A. Svilans, A. M. Burke, E. A. Hoffmann, S. Fahlvik, C. Thelander, M. Leijnse, H. Linke, *Nat. Nanotechnol.* **13**, 920 (2018)
- [11] J. L. D. de Oliveira, M. Rojas, C. Filgueiras, *Phys. Rev. E* **104**, 014149 (2021)
- [12] M. L. Bera, M. Lewenstein, M. N. Bera, *npj Quantum Information* **7**, 4430 (2021)
- [13] S. Çakmak, F. Altintas, *Quantum Information Proc.* **19**, 248 (2020)
- [14] F. J. Peña, O. Negrete, N. Cortés, P. Vargas, *Entropy* **22**, 755 (2020)
- [15] D. Gelbwaser-Klimovsky, A. Bylinskii, D. Gangloff, R. Islam, A. Aspuru-Guzik, V. Vuletic, *Phys. Rev. Lett.* **120**, 170601 (2018)
- [16] X.-L. Huang, X.-Y. Viu, X.-M. Viu, X.-X. Yi, *Eur. Phys. J. D* **68**, 32 (2014)
- [17] S. Çakmak, *J. Opt. Soc. Am. B* **39**, 1209 (2022)
- [18] C. Cruz, H.-R. Rastegar-Sedeqi, M. Anka, T. R. de Oliveira, M. Reis, *Quant. Science Tech.* **8**, 035010 (2023)
- [19] T. R. de Oliveira, D. Jonathan, *Phys. Rev. E*, **104**, 044133 (2021).
- [20] A. El Makouri, A. Slaoui, M. Daoud, *J. Phys. B: At. Mol. Opt. Phys.* **56**, 085501 (2023).
- [21] Y. Yin, L. Chen, F. Wu, Y. Ge, *Physica A* **547**, 123856 (2020)
- [22] M. Y. Abd-Rabbou, A. ur Rahman, M. A. Yurischev, S. Haddadi, *Phys. Rev. E* **108**, 034106 (2023)
- [23] M. Asadian, S. Ahadpour, F. Mirmasoudi, *Sci. Rep.* **12**, 7081 (2022)
- [24] J. Z. He, J. C. Chen, B. Hua, *Phys. Rev. E* **65**, 036145 (2002).
- [25] C. M. Bender, D. C. Body, B. K. Meister, *J. Phys A* **33**, 4427 (2000), J. Wang, Z. Wu, J. He, *Phys. Rev. E* **85**, 041148 (2012).
- [26] E. Aydingir, S. D. Han, *Physica A*, **509**, 766 (2018).
- [27] K. Klinar, M.M. Rojo, Z. Kutnjak, A. Kitanovski, *J. Appl. Phys.* **127**, 234101 (2020)
- [28] V. Chaudhary, Z. Wang, A. Ray, I. Sridhar, R.V. Ramanujan, *J. Phys. D* **50**, 03LT03 (2017)
- [29] M.S. Pattanaik, S.K. Cheekati, V.B. Varma, R.V. Ramanujan, *App. Therm. Eng.* **201**, 117777 (2022)
- [30] U. Sen, S. Chatterjee, S. Sen, M. K. Tiwari, A. Mukhopadhyay, R. Ganguly, *J. Magn. Magn. Mater.* **421**, 165 (2017)
- [31] M. Qian, X. Zhang, L. Wei, P. Martin, J. Sun, L. Geng, T. B. Scott, H.-X. Peng, *Scientific Reports* **8**, 16574 (2018)
- [32] D.N. Ba, L. Becerra, N. Casaretto, J.E. Duvauchelle, M. Marangolo, S. Ahmim, M. Almanza, M. LoBue, *AIP Adv.* **10**, 035110 (2020).
- [33] D.N. Ba, Y.L. Zheng, L. Becerra, M. Marangolo, M. Almanza, M. LoBue, *Phys. Rev. Appl.* **15**, 064045 (2021)
- [34] X.L. Liu, Y.F. Zhang, Y.Y. Wang, W.J. Zhu, G.L. Li, X.W. Ma, Y.H. Zhang, S.Z. Chen, S. Tiwari, K.J. Shi, S.W. Zhang, H.M. Fan, Y.X. Zhao, X.J. Liang, *Theranostics* **10**, 3793 (2020)
- [35] J.B. Li, Y. Qu, J. Ren, W.Z. Yuan, D.L. Shi, *Nanotechnology* **23**, 505706 (2012)
- [36] K.-Y. Choi, Y. H. Matsuda and H. Nojiri, *Phys. Rev. Lett.* **96**, 107202 (2006)
- [37] M. Trif, F. Troiani, D. Stepanenko, and D. Loss, *Rev. Lett.* **101**, 217201 (2008)
- [38] K.-Y. Choi, N. S. Dalal, A. P. Reyes, P.L. Kuhns, Y. H. Matsuda, H. Hojiri, S. S. Mal and U. Kortz, *Phys. Rev. B* **77**, 024406 (2008)
- [39] K.-Y. Choi, Z. Wang, H. Nojiri, J. van Tol, P. Kumar, P. Lemmens, B. S. Bassil, U. Kortz, and N. S. Dalal, *Phys. Rev. Lett.* **108**, 067206 (2012)
- [40] E. T. Spielberg, A. Gilb, D. Plaul, D. Geibig, D. Hornig, D. Schuch, A. Buchholz, A. Ardavan, W. Plass, *Inorg. Chem.* **54**, 3432 (2015)
- [41] M. I. Belinsky, *Inorg. Chem.* **55**, 4091 (2016)
- [42] J. Robert, N. Parizel, P. Turek, A. K. Boudalis, *Phys. Chem. Phys.* **21**, 19575 (2019)
- [43] A. K. Boudalis, *Chem. Eur. J.* **27**, 7022 (2021)
- [44] A. C. Stowe, S. Nellutla, N. S. Dalal, U. Kortz, *Eur. J. Inorg. Chem.* **2004**, 3792 (2004)
- [45] U. Kortz, S. Nellutla, A. C. Stowe, N. S. Dalal, J. van Tol, B. S. Bassil, *Inorg. Chem.* **43**, 144 (2004)
- [46] T. Yamase, E. Ishikawa, K. Fukaya, H. Nojiri, T. Taniguchi, T. Atake, *Inorg. Chem.* **43**, 8150 (2004)
- [47] M.-A. Bouammali, N. Suaud, N. Guihéry, R. Maurice, *Inorg. Chem.* **61**, 12138 (2022)
- [48] P. Kowalewska, K. Szałowski, *J. Magn. Magn. Mater.* **496**, 165933 (2020)
- [49] K. Karlova, J. Strečka, J. Richter, *J. Phys.: Condens. Matter* **29**, 125802 (2017)
- [50] J. Torrico, J. A. Plascak, *Phys. Rev. E* **102**, 062116 (2020)
- [51] J. Torrico, J. A. Plascak, *J. Magn. Magn. Mater.* **552**, 169151 (2022)
- [52] G. A. Antonio, J. Torrico, A. S. da Mata, S. M. de Souza, O. Rojas, *Phys. Rev. B* **108**, 134415 (2023)
- [53] H. T. Quan, P. Zhang, C. P. Sun, *Phys. Rev. E* **72**,

056110 (2005).

[54] D. Das, G. Thomas, A. N. Jordan, *Phys. Rev. A* **108**, 012220 (2023).